Monsoon-induced biases of climate models over the tropical Indian Ocean

Gen Li*

State Key Laboratory of Tropical Oceanography, South China Sea Institute of Oceanology, Chinese Academy of Sciences, Guangzhou, Guangdong, China

Shang-Ping Xie

Scripps Institution of Oceanography, University of California San Diego, La Jolla, California, USA; Physical Oceanography Laboratory, Ocean University of China, Qingdao, Shandong, China

Yan Du

State Key Laboratory of Tropical Oceanography, South China Sea Institute of Oceanology, Chinese Academy of Sciences, Guangzhou, Guangdong, China

**Corresponding author address*: Gen Li, State Key Laboratory of Tropical Oceanography, South China Sea Institute of Oceanology, CAS, 164 West Xingang Road, Guangzhou 510301, China. Email: ligen@scsio.ac.cn

ABSTRACT

Long-standing biases of climate models limit the skills of climate prediction and projection. Overlooked are tropical Indian Ocean (IO) errors. Based on the Coupled Model Intercomparison Project Phase 5 (CMIP5) multi-model ensemble, the present study identifies a common error pattern in climate models that resembles the IO Dipole (IOD) mode of interannual variability in nature, with a strong equatorial easterly wind bias during boreal autumn accompanied by physically consistent biases in precipitation, sea surface temperature (SST), and subsurface ocean temperature. The analyses show that such IOD-like biases can be traced back to errors in the South Asian summer monsoon. Too weak a southwest summer monsoon over the Arabian Sea generates a warm SST bias over the western equatorial IO. In boreal autumn, Bjerknes feedback helps amplify the error into an IOD-like bias pattern in wind, precipitation, SST, and subsurface ocean temperature. Such mean state biases result in too strong interannual IOD variability. Most models project an IOD-like future change for the boreal autumn mean state in the global warming scenario, which would result in more frequent occurrences of extreme positive IOD events in the future with important consequences to Indonesia and East Africa. The Intergovernmental Panel on Climate Change (IPCC) Fifth Assessment Report (AR5) characterizes this future IOD-like projection in the mean state as robust based on consistency among models, but our results cast doubts on this conclusion since models with larger IOD amplitude biases tend to produce stronger IOD-like projected changes in the future.

1. Introduction

The tropical Indian Ocean (IO), in contrast to the tropical Pacific and Atlantic Oceans, features a unique monsoonal climate (Schott et al. 2009) where the Asian continent drives the strongest monsoon on Earth (e.g., Li and Yanai 1996; Lau et al. 2006; Boos and Kuang 2010) and the cross-equatorial monsoonal winds display the dramatic seasonal reversals. The interaction of the South Asian monsoon with the ocean plays an important role in shaping the regional climate in many ways. For instance, the monsoonal winds bring about large seasonal alternations in ocean currents such as the annual reversal of the Somali Current in the Arabian Sea (Schott and McCreary 2001; Schott et al. 2002). Momentum advection by the cross-equatorial monsoon circulation drives the semiannual cycle in equatorial IO zonal wind (Ogata and Xie 2011). As a result, the oceanic Wyrtki jets carry warm upper-layer waters eastward twice a year in the equatorial IO during the inter-monsoon periods (Wyrtki 1973; Schott et al. 2009). Such monsoon-induced characteristics are unique to the IO, and climatically important on both regional and global scales. The seasonal development of the southeasterly alongshore wind off Indonesia locks the IO Dipole (IOD) mode of inter-annual variability to boreal summer-autumn (Saji et al. 1999; Webster et al. 1999; Murtugudde et al. 2000; Yamagata et al. 2004; Du et al. 2013), a phenomenon of profound social and economic consequences for the IO rim countries (e.g., Ashok et al. 2001; Guan and Yamagata 2003; Hashizume et al. 2009; Cai et al. 2009; Ummenhofer et al. 2011; Weller and Cai 2013a).

Unfortunately, many coupled general circulation models (CGCMs) exhibit large biases in the South Asian summer monsoon, with the upper-tropospheric temperature maximum over Tibet being too weak and displaced southeast of its observed location (Boos and Hurley 2013) along with insufficient summer precipitation over the South Asian monsoon region (e.g., Annamalai et al. 2007). However, it is unclear how these monsoon biases influence regional climate simulation and projection beyond the monsoon itself.

CGCMs suffer from serious errors in simulating tropical Pacific and Atlantic climate, including an excessive equatorial cold tongue in the Pacific (e.g., Neelin et al. 1992; Mechoso et al. 1995; Yu and Mechoso 1999; Davey et al. 2002; Wittenberg et al. 2006; de Szoeke and Xie 2008; Zheng et al. 2012; Li and Xie 2014), too weak a zonal sea surface temperature (SST) gradient along the equatorial Atlantic (e.g., Davey et al. 2002; Chang et al. 2007; Richter and Xie 2008; Wahl et al. 2011; Grodsky et al. 2012; Liu et al. 2013; Kozar and Misra 2013), and too warm SSTs over the tropical Southeast Pacific and Atlantic accompanied by a spurious double intertropical convergence zone (e.g., Mechoso et al. 1995; Zhang and Wang 2006; Lin 2007; Song and Zhang 2009; Hwang and Frierson 2013; Li and Xie 2014; Wang et al. 2014). These long-standing tropical biases exist in several generations of CGCMs for more than a decade, including those participating in the Coupled Model Intercomparison Project Phase 5 (CMIP5; Taylor et al. 2012; Hwang and Frierson 2013; Li and Xie 2014; Wang et al. 2014).

Tropical IO biases in CGCMs are previously overlooked to a large extent, for one important reason. Annual mean biases may be small in magnitude in the tropical IO relative to other two tropical basins (e.g., Lin 2007; Hwang and Frierson 2013; Li and Xie 2014; Wang et al. 2014), but as will be described, the tropical IO biases have strong seasonal dependence with even seasonal sign reversals in wind/SST, resulting in small annual means. Recently, Lee et al. (2013) identified a common annual mean easterly wind bias along the equatorial IO in state-of-the-art CGCMs participating in both the CMIP3 and CMIP5. Cai and Cowan (2013) further found that the annual mean equatorial easterly wind bias in CGCMs is accompanied by an overly strong west-minus-east SST gradient and the unrealistic climatological mean thermocline slope tilting upward toward the eastern equatorial IO, suggestive of the positive ocean-atmospheric feedback of Bjerknes (1969).

Although previous studies have noticed some annual mean simulation errors in the equatorial IO in CGCMs, many issues remain unresolved. For example, since the oceanic and atmospheric fields are closely coupled in the positive Bjerknes feedback loop and errors in one field will propagate into all the elements in the loop as a "chicken and egg" problem, it is unclear which element initiates the development of such equatorial IO biases. The seasonal evolutionary characteristics/processes of equatorial IO biases have not been studied. Moreover, the bias pattern off the equator is unknown. In particular, it is also unclear whether the equatorial IO biases are associated with errors of the South Asian summer monsoon. There are physical

reasons for the South Asian monsoon affecting equatorial IO biases. For example, the cross-equatorial monsoonal winds could affect SST in the western equatorial IO because of oceanic upwelling near, and heat advection from, the Somali and Omani coasts and of latent heat loss caused by the strong surface winds (Schott and McCreary 2001; Izumo et al. 2008; Schott et al. 2009). In addition, the meridional momentum advection during the monsoonal periods could affect the strength of westerly winds along the equator (Ogata and Xie 2011).

The present study investigates seasonally dependent biases over the tropical IO in 19 CMIP5 CGCMs. Our analysis reveals pronounced biases during boreal autumn (September-November, SON) organized in coherent IOD-like patterns with a strong equatorial easterly wind bias accompanied by physically consistent biases in precipitation, SST, and subsurface ocean temperature. We show that these coupled ocean-atmosphere biases originate from too weak a southwest monsoon over the Arabian Sea during boreal summer (June-August, JJA) and the resultant warm SST bias in the western equatorial IO. In SON, the SST error is amplified into an IOD-like bias pattern through Bjerknes feedback. These mean state biases result in too large an amplitude of interannual IOD variability and also distort future climate projection in the region. In particular, models with larger IOD amplitude biases tend to project stronger IOD-like future changes. Our study highlights the tropical IO errors in CGCMs and emphasizes the importance of a realistic South Asian monsoon

simulation for reducing tropical IO simulation errors for both mean state and climate variability as well as increasing the reliability of regional future climate projection.

The remainder of this paper is organized as follows. In Section 2, we provide a brief description of the models, datasets, and methods used in this study. Section 3 introduces the annual mean IOD-like biases over the tropical IO in the CMIP5 multi-model ensemble. Section 4 further investigates the seasonal development processes of IOD-like biases and their South Asian summer monsoon origin. Section 5 discusses the effects of such IOD-like mean state biases on the simulation of tropical IO interannual variability and regional climate projection under global warming. Section 6 is a summary.

2. Models, datasets, and methods

We examine the historical and RCP 8.5 experiments in the CMIP5 multi-model ensemble (Taylor et al. 2012). Monthly mean outputs from 19 CMIP5 CGCMs are used, including precipitation, wind and geopotential height at lower troposphere (925 mb), SST, and ocean temperature. Table 1 shows the model names, modeling groups (or centers), and their letter labels. Further information on individual models is available online at http://www-pcmdi.llnl.gov/ (Taylor et al. 2012). Here, we only use one ensemble member (‘‘r1i1p1’’) run for each model. The 1950-1999 mean in historical simulations is represented as the present climatology, and the 2050-2099 mean in Representative Concentration Pathway (RCP) 8.5 runs as the future

climatology. Their difference denotes climate change under global warming. The multi-model ensemble mean (MME) bias in this study is defined as the difference between the 19 model mean and observations, unless otherwise specified.

For comparison, we also examine both the observed and reanalyzed (assimilated) datasets (for simplicity referred to as observations). Specifically, the precipitation climatology is obtained from the Global Precipitation Climatology Project (GPCP; Adler et al. 2003) for 1979-2008 and from the National Center for Atmospheric Research-National Centers for Environmental Prediction (NCEP-NCAR) reanalysis project (Kalnay et al. 1996) for 1950-1999. Although the two precipitation products cover different time periods, the climatology is very similar. Only the results from the GPCP are shown, unless otherwise specified. The wind and geopotential height in the lower troposphere (925 mb) is the climatology from ECWMF 40 Year Re-analysis (ERA-40) (Uppala et al. 2005) for 1958-2001. The SST climatology is obtained from Hadley Centre Sea Ice and SST (HadISST; Rayner et al., 2003) for 1950-99. In addition, the ocean temperature from the Simple Ocean Data Assimilation (SODA) reanalysis (Carton and Giese 2008) from 1950 to 1999 is used. All model outputs and observational datasets are interpolated to a uniform $2° \times 2°$ horizontal grid, unless otherwise specified.

To examine the inter-model diversity of seasonal mean SST (or wind) biases, we perform an inter-model empirical orthogonal function (EOF) analysis for observations and 19 CMIP CGCMs. Instead of temporal variance in conventional EOF analysis

(Hannachi et al. 2007), our inter-model EOF analysis maximizes the variance of inter-model differences in SST (or wind) biases among CMIP5 CGCMs. For example, the two dimensional space-model filed of SST biases, SST(m, s), is expanded into K orthogonal spatial patterns as follows:

$$\mathrm{SST}(m,s) = \sum_{k=1}^{\mathrm{K}} \mathrm{u}_k(s)\mathrm{a}_k\,(m) \qquad (1)$$

where s and m denote spatial position (latitude-longitude) and different models, respectively; u_k is the vector which gives the spatial structure of the mode of inter-model variances in SST biases; a_k is corresponding model coefficients in SST biases. The inter-model EOF method has been successfully used for the tropical oceans (Li and Xie 2012, 2014) and extratropical oceans (Wang et al. 2014).

3. Annual mean biases

Figure 1 compares the annually averaged zonal wind, precipitation, and SST along the equatorial IO between observations (black lines) and 19 CMIP5 CGCMs (colored lines). Although the zonal distributions of annual mean zonal wind, precipitation, and SST along the equatorial IO are qualitatively simulated, large errors are clearly found in the CMIP5 CGCMs. For example, annual mean equatorial westerly winds are too weak in most CMIP5 CGCMs relative to observations (Figure 1a; Lee et al. 2013; Cai and Cowan 2013). Also, the CMIP5 CGCMs commonly simulate the excessive (slightly insufficient) precipitation in the western (eastern) equatorial IO (Figure 1b).

Figures 2a and 2b show the spatial patterns of annual mean wind, precipitation, and SST over the tropical IO (40°-110°E, 20°S-20°N) for observations and the MME biases in CMIP5 CGCMs, respectively. Here, we focus on the spatial distributions of model biases by normalizing with the tropical IO means of precipitation and SST for observations and each model. Indeed, the CMIP5 CGCMs suffer from a strong equatorial easterly wind bias accompanied by excessive (insufficient) precipitation in the western (eastern) basin (Figure 2b), in patterns similar to a positive IOD event (Saji et al. 1999) in nature. In particular, annual mean southwesterly (southeasterly) winds over the North (South) IO are significantly weaker in CMIP5 CGCMs than observations. Such annual mean IOD-like biases on the equator and weakened southwesterly (southeasterly) winds over the North (South) IO are present in most CMIP5 CGCMs (see Figure S1 in the Supplementary Material).

For annual mean, the bias in west-east SST gradient along the equatorial IO seems weak (Figures 1c and 2b), and does not match well with wind and precipitation biases in an IOD-like manner. Figures 3a, 3b, 3c, and 3d show the MME biases of seasonally averaged SST in CMIP5 CGCMs relative to observations during boreal spring (March-May, MAM), JJA, SON, and boreal winter (December-February, DJF), respectively. A close inspection reveals extremely warm (slightly cool) SST biases in the western (eastern) IO in both JJA and SON, suggestive of a positive IOD-like bias.

Figures 4a, 4b, and 4c show the equatorial IO zonal wind, precipitation, and SST during June-November in observations (black lines) and 19 CMIP5 CGCMs (colored

lines), respectively. The seasonal biases of zonal wind and precipitation along the equator in CGCMs are more pronounced than their annual mean biases (Figures 1 and 4). While observations display robust equatorial westerly winds (Figure 4a) as a part of the Walker circulation (Schott et al. 2009), half of the CGCMs feature easterly winds on the equator (Figure 4a). In addition, almost all CGCMs exhibit warm SST biases in the equatorial western IO, implying seasonally dependent biases in west-minus-east SST gradient (Figure 4c).

4. Seasonal cycle of errors and the monsoon origin

a. Seasonal cycle of errors

To show the seasonality of the biases, Figure 5 compares the longitude-time sections of 925 mb wind, precipitation, and SST along the equatorial IO between observations and the MME simulation. The weakened cross-equatorial JJA monsoon causes a strong warm SST bias in the west (Figure 5b). While the MME bias in cross-equatorial winds is no longer significant in September, the SST error in the equatorial western IO could last till November-December when an overly strong cross-equatorial boreal winter monsoon reverses the sign of SST bias (Figure 5b). The seasonal sign reversal in SST bias renders the annual mean small on the equator. While the warm SST bias occurs in both JJA and SON over the western equatorial IO, the easterly wind bias along the equator and excessive precipitation in the western equatorial IO in CMIP5 CGCMs are much more pronounced in SON than JJA.

Associated with the equatorial easterly wind bias, the models tend to display an overly steep slope in the thermocline depth (20 °C isotherm, Z20) shoaling towards the east. Figure 6 shows the ocean temperature structures in the zonal-vertical plane along the equator during SON in observations and the MME simulation. Indeed, models generally feature a too steep eastward shoaling of Z20 in the equatorial eastern IO during SON. Most CMIP5 CGCMs share such an unrealistic equatorial Z20 slope tilting upward toward the east (see Figure S2 in the Supplementary Material). This relationship among wind, precipitation, SST, and z20 biases during SON (Figures 5b and 6b) is suggestive of Bjerknes feedback.

These results are supported by an inter-model analysis. We perform an inter-model EOF analysis for JJA SST and SON zonal wind separately in the equatorial IO (40°-100°E, 6°S-6°N) among observations and 19 CMIP5 CGCMs. The SST for observations and each CGCM is normalized by their tropical IO means. The first modes (Figures 7a and 7b) feature a JJA SST zonal dipole and SON easterly wind biases along the equatorial IO, respectively. The first principal component (PC1) for JJA SST is highly correlated with the west-east SST gradient along the equatorial IO (40°-60°E minus 80°-100°E) in JJA at 0.82 (Figure 7c), while the SON wind PC1 with zonal wind in the central equatorial IO (CEIO, 70°-90°E) in SON at -0.99 (Figure 7e). Furthermore, the two PC1s are mutually correlated at 0.63 (Figure 7f), suggesting that the JJA west-east SST gradient bias drives the SON equatorial easterly wind bias.

b. Errors in JJA versus SON

Then, why do the IOD-like coupled biases develop in SON instead of in JJA? Although the warm SST bias in the western equatorial IO is present as early as in JJA, the equatorial easterly wind bias does not develop until SON (Figure 5b). Figures 8a and 8b examine the relationship between the west-east SST gradient along the equatorial IO and CEIO zonal wind among observations and 19 CMIP5 CGCMs for JJA and SON, respectively. There is a strong inter-model correlation (r=-0.92) between the west-minus-east SST gradient and CEIO zonal wind biases in SON, but this inter-model relationship is insignificant in JJA (r=-0.22), suggesting that the positive Bjerknes feedback loop is broken in JJA.

The zonal momentum equation on the equator within the planetary boundary layer (generally below 850 mb) can be written approximately as (Okumura and Xie 2004; Ogata and Xie 2011):

$$\varepsilon u = -\frac{\partial \Phi}{\partial x} - v\frac{\partial u}{\partial x} + \text{res.}, \qquad (2)$$

where ε is the linear drag coefficient, *u* is the zonal wind, the first term on the right hand side is the pressure gradient, the second term is the meridional momentum advection, and the last term is the residual. In JJA, the advection of the easterly momentum from the southeast trades by the southerly cross-equatorial wind is important in the equatorial IO (Ogata and Xie 2011). For CGCMs, the weakened cross-equatorial monsoon wind bias in JJA warms SST in the western IO, and the

resultant west-east SST/pressure gradient would induce equatorial easterly wind bias. The weakened cross-equatorial southerly wind at the same time reduces the easterly momentum advection, opposing the SST/pressure gradient effect. Thus, the two effects of the cross-equatorial wind bias are out of phase, precluding a strong relationship between the SST gradient and zonal wind biases in JJA (Figure 8a).

We test this hypothesis by examining the pressure gradient and meridional momentum advection terms in Equation (2). Figures 9a and 9b show the longitude-time sections of MME biases for the pressure gradient and meridional momentum advection terms along the equatorial IO in 19 CMIP5 CGCMs, respectively. Indeed, the SST/pressure effect in JJA is to generate easterly wind bias, particularly in the western equatorial IO, but the meridional momentum advection effect is large and offsets the SST/pressure effect. In SON, with the monsoon gone, the SST/pressure effect prevails and induces the easterly wind bias over the CEIO, allowing Bjerknes feedback to develop the IOD-like biases rapidly. This has more or less implications for the important question of why the observed IOD events generally peak in SON rather than in JJA (e.g., Saji et al. 1999; Webster et al. 1999; Cai and Cowan 2013).

c. Monsoon origin

Figures 10a and 10b show the spatial distributions of MME biases of 925 mb wind, precipitation, and SST over the tropical IO in CMIP5 CGCMs during JJA and

SON, respectively. The southwest monsoon in JJA is too weak in CMIP5 CGCMs over the Arabian Sea along with insufficient summer precipitation over the South Asian monsoon region. The weakened cross-equatorial monsoon generates warm SST and excessive precipitation biases over the western equatorial IO (Figure 10a). The warm SST bias in the equatorial western IO persists until SON, when Bjerknes feedback helps amplify the SST error into an IOD-like bias pattern with a strong equatorial easterly wind bias accompanied by warm (cool) SST and excessive (insufficient) precipitation biases in the western (eastern) basin (Figure 10b).

Inter-model statistics also support the hypothesis that the seasonally dependent IOD-like biases are induced by biases of the South Asian summer monsoon. Figures 11a and 11b show the relationship between the cross-equatorial meridional wind in the western IO (40°-60°E) and west-minus-east SST gradient along the equatorial IO in JJA, and between the west-minus-east SST gradients along the equatorial IO in JJA and SON, respectively. Models with a weaker cross-equatorial monsoon in JJA tend to develop larger equatorial SST gradient biases in both JJA and SON, suggesting the importance of a good JJA monsoon simulation for improving SST simulation during JJA and SON. The SST gradient bias then induces the equatorial easterly wind error in SON (Figure 8b). The easterly wind bias steepens the z20 slope along the equatorial IO (Figure 11c), which in turn helps intensify the SST gradient bias (Figure 11d). Figure 12 summarizes the South Asian monsoon origin and Bjerknes feedback for the IOD-like bias pattern.

5. Discussion on regional climate variability and change

The CMIP5 CGCMs have been used for global climate simulation and projection on a lot of aspects (e.g., Taylor et al. 2012; Christensen et al. 2013). However, long-standing biases of mean state simulation for the equatorial Pacific cold tongue and intertropical convergence zone (ITCZ) considerably limit the skills of CGCMs in simulating and predicting El Nino-Southern Oscillation (ENSO) as well as its global teleconnections (Latif et al. 2001; Guilyardi 2006; AchutaRao and Sperber 2006; Wittenberg et al. 2006; Misra et al. 2008; Ham and Kug 2012; Li and Xie 2014). Conceivably a realistic simulation of tropical IO mean state by the CMIP5 CGCMs is also an important prerequisite for their good skill in regional climate simulation and projection.

We turn our attention to the effects of such IOD-like mean state biases on the simulation of tropical IO interannual variability and regional climate projection under global warming. With the equatorial easterly wind bias, the unrealistically steep equatorial Z20 slope tilting upward toward the eastern IO during SON (Figure 6) generates an overly strong subsurface thermocline feedback on SST, helping develop an excessively large amplitude of interannual IOD variability in CGCMs (Cai and Cowan 2013; Liu et al. 2014). Figure 13a compares the amplitudes of interannual IOD variability between observations and the MME simulation as a function of calendar month. In this study, the IOD amplitude is defined as the standard deviation

of the Dipole Mode index (DMI) proposed by Saji et al. (1999). The error bars indicate the standard deviation spread among 19 CMIP5 CGCMs. Indeed, CMIP5 CGCMs tend to produce too large an IOD amplitude, twice as large for the MME simulation compared to observations in the IOD peak-season.

Our recent research (Li et al. 2015) suggests that this typical easterly wind error along the equatorial IO could induce too deep a thermocline dome over the southwestern IO (SWIO) in CGCMs by forcing a westward-propagating downwelling Rossby wave in the tropical South IO, extremely similar to a South IO oceanic Rossby wave response to El Nino-forced equatorial easterly wind anomalies in nature (Xie et al. 2002; Du et al. 2009). Due to the deep thermocline bias over the SWIO, too weak a thermocline feedback on SST there leads to a suppressed simulation amplitude of interannual variability for the IO basin (IOB; Klein et al. 1999; Lau et al. 2000) mode in CGCMs and possibly limits the CGCMs' skill in predicting the IOB warming following El Nino and extreme climate and weather events over the IO and rim countries/regions such as East Asia affected by the IOB (Yang et al. 2007; Xie et al. 2009; Kosaka et al. 2013; Li et al. 2015).

Most CGCMs project an IOD-like pattern of coupled ocean-atmospheric climate changes in the SON mean state over the tropical IO under global warming, with equatorial easterly wind anomalies (i.e., a weakened tropical Walker circulation; Knutson and Manabe 1995; Held and Soden 2006; Vecchi and Soden 2007) as well as physically consistent west-east SST gradient, the precipitation dipole, and the

shoaling thermocline in the equatorial eastern IO (Zheng et al. 2010, 2013; Cai et al. 2013). This climate change pattern has important consequences to the IO and its surrounding countries (Saji et al. 1999; Hashizume et al. 2009; Weller and Cai 2013a, 2013b; Cai et al. 2014). For example, attributed to such an IOD-like future change for the mean state in the global warming scenario, the CMIP5 ensemble of CGCMs forced by a scenario of high greenhouse gas emissions (RCP 8.5 runs) commonly projects an increased frequency of extreme positive IOD events by almost three times from about one event every 17 years during the twentieth century to about one event every 6 years during the twenty-first century (Cai et al. 2014), with an increasing risk of extreme climate and weather events over Indonesia and East Africa (Saji et al. 1999; Hashizume et al. 2009; Weller and Cai 2013a, 2013b).

In particular, the Intergovernmental Panel on Climate Change (IPCC) Fifth Assessment Report (AR5) characterized this IOD-like projected pattern in the SON mean state as robust based on the consistency among climate models (Christensen et al. 2013), but our results cast doubts on this conclusion since CGCMs tend to feature too strong a Bjerknes feedback in SON that produces the IOD pattern in the first place. Figure 13b examines the relationship between the simulated present IOD amplitude and projected zonal wind change over the CEIO for SON under global warming among 19 CMIP5 CGCMs. The red line denotes the observed amplitude of interannual IOD variability. Indeed, models with a larger present IOD amplitude bias tend to generate a stronger IOD-like change pattern of future climate in equatorial IO

zonal wind for SON in the context of global warming, and the corresponding inter-model correlation reaches -0.82 with one outlier (M2) excluded. The similar inter-model spread relationship between the present-day IOD amplitude simulation and projected SST/precipitation dipole change in the future can be also found (not shown; Weller and Cai 2013b). In fact, the projected IOD-like mean state future change in equatorial IO zonal wind for SON under global warming would be not significant (nearly zero change in CEIO zonal wind; see Figure 13b) after calibrating the present-day climate simulation to observations in light of such a strong inter-model spread linear correlation between the present-day IOD amplitude simulation bias and future IOD-like climate projection. Considering the South Asian summer monsoon origin of the biased tropical IO mean state and exaggerated IOD amplitude in CMIP5 CGCMs (Figure 12), the present work implies that reducing JJA monsoon simulation errors would potentially increase our confidence for the reliability of regional future climate projections by CGCMs.

6. Summary

The tropical IO is unique in its strong interaction with the great monsoon of South Asia. The southwest summer monsoon is too weak over the Arabian Sea in most CMIP5 models. This monsoon bias creates a warm SST bias over the western equatorial IO. In SON, Bjerknes feedback kicks in to amplify biases into an IOD-like pattern, with easterly wind errors and a too steep eastward shoaling of the thermocline

in the equatorial IO (Figure 12). The seasonally dependent biases in the mean state affect inadvertently the simulation of interannual variability and projection of future climate in the region. Specifically, the excessive shoaling of the thermocline in the eastern equatorial IO causes too strong a Bjerknes feedback, resulting in an excess in the amplitude of inter-annual IOD variability. While the inter-model consistency led the IPCC AR5 to conclude that the future IOD-like climate change is robust, our results cast doubts on the reliability of this mean state future projection since models tend to exaggerate Bjerknes feedback that produces the IOD pattern in the first place. Such an IOD-like future change in the mean state is climatically important, which would result in more frequent occurrences of extreme positive IOD events in the future (Cai et al. 2014), with a potentially increasing risk of extreme climate and weather events in the regions affected by the IOD such as Indonesia and East Africa (Saji et al. 1999; Hashizume et al. 2009; Weller and Cai 2013a, 2013b).

This example illustrates the need for model evaluation to go beyond simple performance metrics like the annual mean SST but to assess physical processes like Bjerknes feedback. In the monsoonal IO, mutually consistent representation of ocean-land-atmospheric processes and their interactions is key to improving climate models. The benefits of improved seasonal prediction and regional climate projection are enormous for more than a billion people living under the monsoon and affected by the IO.

Acknowledgments. This work was supported by the National Basic Research Program of China (Grants 2012CB955603 and 2010CB950302), the Natural Science Foundation of China (Grant 41406026), the Pearl River Nova Program of Guangzhou, the Technology Foundation for Selected Overseas Chinese Scholars (Ministry of Human Resources and Social Security of the People's Republic of China), the US National Science Foundation, and the CAS/SAFEA International Partnership Program for Creative Research Teams. The authors are grateful to Dr. Riyu Lu for helpful comments. We also wish to thank the climate modeling groups (Table 1) for producing and making available their model output, the WCRP's Working Group on Coupled Modeling (WGCM) for organizing the CMIP5 analysis activity, the Program for Climate Model Diagnostics and Intercomparison (PCMDI) for collecting and archiving the CMIP5 multi-model data, and the Office of Science, U.S. Departmentof Energy for supporting these datasets in partnership with the Global Organization for Earth System Science Portals.

REFERENCES

AchutaRao, K., and K. R. Sperber, 2006: ENSO simulation in coupled ocean-atmosphere models: Are the current models better? *Climate Dyn.,* **27,** 1–15.

Adler, R. F., and Coauthors, 2003: The version 2 global precipitation climatology project (GPCP) monthly precipitation analysis (1979-present). *J. Hydrometeor.,* **4,** 1147–1167.

Annamalai, H., K. Hamilton, and K. R. Sperber, 2007: The South Asian summer monsoon and its relationship with ENSO in the IPCC AR4 simulations. *J. Climate,* **20,** 1071–1092.

Ashok, K., Z. Guan, and T. Yamagata, 2001: Impact of the Indian Ocean dipole on the relationship between the Indian monsoon rainfall and ENSO. *Geophys. Res. Lett.,* **28,** 4499–4502.

Bjerknes, J., 1969: Atmospheric teleconnections from the equatorial Pacific. *Mon. Wea. Rev.,* **97,** 163–172.

Boos, W. R., and Z. Kuang, 2010: Dominant control of the South Asian monsoon by orographic insulation versus plateau heating. *Nature,* **463,** 218–223.

Boos, W. R., and J. V. Hurley, 2013: Thermodynamic bias in the multimodel mean boreal summer monsoon. *J. Climate,* **26,** 2279–2287.

Cai, W., and T. Cowan, 2013: Why is the amplitude of the Indian Ocean Dipole overly large in CMIP3 and CMIP5 climate models? *Geophys. Res. Lett.,* **40,** 1200–1205.

Cai, W., T. Cowan, and M. Raupach, 2009: Positive Indian Ocean Dipole events precondition southeast Australia bushfires. *Geophys. Res. Lett.,* **36,** L19710, doi:10.1029/2009GL039902.

Cai, W., X.-T. Zheng, E. Weller, M. Collins, T. Cowan, M. Lengaigne, W. Yu, and T. Yamagata, 2013: Projected response of the Indian Ocean Dipole to greenhouse warming. *Nature Geosci.,* **6,** 999–1007.

Cai, W., A. Santoso, G. J. Wang, E. Weller, L. Wu, K. Ashok, Y. Masumoto, and T. Yamagata, 2014: Increased frequency of extreme Indian Ocean Dipole events due to greenhouse warming. *Nature,* **510,** 254–258.

Carton, J. A., and B. S. Giese, 2008: A reanalysis of Ocean climate using simple Ocean data assimilation (SODA). *Mon. Wea. Rev.,* **136,** 2999–3017.

Chang, C. Y., J. A. Carton, S. A. Grodsky, and S. Nigam, 2007: Seasonal climate of the tropical Atlantic sector in the NCAR Community Climate System Model 3: Error structure and probable causes of errors. *J. Climate,* **20,** 1053–1070.

Christensen, J. H. and Coauthors, 2013: Climate phenomena and their relevance for future regional climate change. In: *Climate Change 2013: The Physical Science Basis. Contribution of Working Group I to the Fifth Assessment Report of the Intergovernmental Panel on Climate Change* [Stocker, T. F. et al. (eds.)].

Cambridge University Press, Cambridge, United Kingdom and New York, NY, USA.

Davey, M. K., and Coauthors, 2002: STOIC: A study of coupled model climatology and variability in tropical ocean regions. *Climate Dyn.,* **18,** 403–420.

de Szoeke, S. P., and S.-P. Xie, 2008: The tropical eastern Pacific seasonal cycle: Assessment of errors and mechanisms in IPCC AR4 coupled ocean-atmosphere general circulation models. *J. Climate,* **21,** 2573–2590.

Du, Y., S.-P. Xie, G. Huang, and K. Hu, 2009: Role of air-sea interaction in the long persistence of El Nino-induced North Indian Ocean warming. *J. Climate,* **22,** 2023–2038.

Du, Y., W.-J. Cai, and Y.-L. Wu, 2013: A new type of the Indian Ocean Dipole since the mid-1970s. *J. Climate*, **26,** 959–972.

Grodsky, S. A., J. A. Carton, S. Nigam, and Y. M. Okumura, 2012: Tropical Atlantic biases in CCSM4. *J. Climate,* **25,** 3684–3700.

Guan, Z., and T. Yamagata, 2003: The unusual summer of 1994 in East Asia: IOD teleconnections. *Geophys. Res. Lett.,* **30**(10), 1544, doi:10.1029/2002GL016831.

Guilyardi, E., 2006: El Nino-mean state-seasonal cycle interactions in a multi-model ensemble. *Climate Dyn.,* **26,** 329–348.

Ham, Y. G., and J. S. Kug, 2012: How well do current climate models simulate two types of El Nino? *Climate Dyn.,* **39,** 383–398.

Hannachi, A., I. T. Jolliffe, and D. B. Stephenson, 2007: Empirical orthogonal functions and related techniques in atmospheric science: A review. *Int. J. Climatol.,* **27,** 1119–1152.

Hashizume, M., T. Terao, and N. Minakawa, 2009: The Indian Ocean Dipole and malaria risk in the highlands of western Kenya. *Proc. Natl. Acad. Sci. USA,* **106,** 1857–1862.

Held, I. M., and B. J. Soden, 2006: Robust responses of the hydrological cycle to global warming. *J. Climate,* **19,** 5686–5699.

Hwang, Y.-T., and D. M. M. Frierson, 2013: Link between the double-intertropical convergence zone problem and cloud biases over the Southern Ocean. *Proc. Natl. Acad. Sci. USA,* **110,** 4935–4940.

Izumo, T., C. Boyer Montegut, J.-J. Luo, S. K. Behera, S. Masson, and T. Yamagata, 2008: The role of the western Arabian Sea upwelling in Indian monsoon rainfall variability. *J. Climate,* **21,** 5603–5623.

Kalnay, E, and Coauthors, 1996: The NCEP/NCAR 40-year reanalysis project. *Bull. Amer. Meteor. Soc.,* **77,** 437–471.

Klein, S. A., B. J. Soden, and N.-C. Lau, 1999: Remote sea surface temperature variations during ENSO: Evidence for a tropical atmospheric bridge. *J. Climate,* **12,** 917–932.

Knutson, T. R., and S. Manabe, 1995: Time-mean response over the tropical Pacific to increased CO2 in a coupled ocean-atmosphere model. *J. Climate,* **8,** 2181–2199.

Kosaka, Y., S.-P. Xie, N.-C. Lau, and G. A. Vecchi, 2013: Origin of seasonal predictability for summer climate over the Northwestern Pacific. *Proc. Natl. Acad. Sci. USA,* **110,** 7574–7579.

Kozar, M. E., and V. Misra, 2013: Evaluation of twentieth-century Atlantic warm pool simulations in historical CMIP5 runs. *Climate Dyn.,* **41,** 2375–2391.

Latif, M., and Coauthors, 2001: ENSIP: The El Niño simulation intercomparison project. *Climate Dyn.,* **18,** 255–276.

Lau, K. M, M. K. Kim, and K. M. Kim, 2006: Asian summer monsoon anomalies induced by aerosol direct forcing: The role of the Tibetan Plateau. *Climate Dyn.,* **26,** 855–864.

Lau, N.-C., and M. J. Nath, 2000: Impact of ENSO on the variability of the Asian-Australian monsoons as simulated in GCM experiments. *J. Climate,* **13,** 4287–4309.

Lee, T., D. E. Waliser, J.-L. F. Li, F. W. Landerer, and M. M. Gierach, 2013: Evaluation of CMIP3 and CMIP5 wind stress climatology using satellite measurements and atmospheric reanalysis products. *J. Climate,* **26,** 5810–5826.

Li, C., and M. Yanai, 1996: The onset and interannual variability of the Asian summer monsoon in relation to land-sea thermal contrast. *J. Climate,* **9,** 358–375.

Li, G., and S.-P. Xie, 2012: Origins of tropical-wide SST biases in CMIP multi-model ensembles. *Geophys. Res. Lett.,* **39,** L22703, doi:10.1029/2012GL053777.

Li, G., and S.-P. Xie, 2014: Tropical biases in CMIP5 multimodel ensemble: The excessive equatorial Pacific cold tongue and double ITCZ problems. *J. Climate,* **27,** 1765–1780.

Li, G., S.-P. Xie, and Y. Du, 2015: Climate model errors over the South Indian Ocean thermocline dome and their effect on the basin mode of interannual variability. *J. Climate,* submitted.

Lin, J.-L., 2007: The double-ITCZ problem in IPCC AR4 coupled GCMs: Ocean-atmosphere feedback analysis. *J. Climate,* **20,** 4497–4525.

Liu, H., C. Wang, S.-K. Lee, and D. B. Enfield, 2013: Atlantic warm pool variability in the CMIP5 simulations. *J. Climate,* **26,** 5315–5336.

Liu, L., S.-P. Xie, X.-T. Zheng, T. Li, Y. Du, G. Huang, and W.-D. Yu, 2014: Indian Ocean variability in the CMIP5 multi-model ensemble: The zonal dipole mode. *Climate Dyn.,* **43,** 1715–1730.

Mechoso, C. R., and Coauthors, 1995: The seasonal cycle over the tropical Pacific in coupled ocean-atmosphere general circulation models. *Mon. Wea. Rev.,* **123,** 2825–2838.

Misra, V., L. Marx, M. Fennessey, B. Kirtman, and J. L. Kinter III, 2008: A comparison of climate prediction and simulation over tropical Pacific. *J. Climate,* **21,** 3601–3611.

Murtugudde, R. G., J. P. McCreary, and A. J. Busalacchi, 2000: Oceanic processes associated with anomalous events in the Indian Ocean with relevance to 1997-1998. *J. Geophys. Res.,* **105,** 3295–3306.

Neelin, J. D., and Coauthors, 1992: Tropical air-sea interaction in general circulation models. *Climate Dyn.,* **7,** 73–104.

Ogata, T., and S.-P. Xie, 2011: Semiannual cycle in zonal wind over the equatorial Indian Ocean. *J. Climate,* **24,** 6471–6485.

Okumura, Y., and S.-P. Xie, 2004: Interaction of the Atlantic equatorial cold tongue and African monsoon. *J. Climate,* **17,** 3588–3601.

Rayner, N. A., D. E. Parker, E. B. Horton, C. K. Folland, L. V. Alexander, D. P. Rowell, E. C. Kent, and A. Kaplan, 2003: Global analyses of sea surface temperature, sea ice, and night marine air temperature since the late nineteenth century. *J. Geophys. Res.,* **108**(D14), 4407, doi:10.1029/2002JD002670.

Richter, I., and S.-P. Xie, 2008: On the origin of equatorial Atlantic biases in coupled general circulation models. *Climate Dyn.,* **31,** 587–598.

Saji, N. H., B. N. Goswami, P. N. Vinayachandran, and T. Yamagata, 1999: A dipole mode in the tropical Indian Ocean. *Nature,* **401,** 360–363.

Schott, F. A., and J. P. McCreary, 2001: The monsoon circulation of the Indian Ocean. *Prog. Oceanogr.,* **51,** 1–123.

Schott, F., M. Dengler, and R. Schoenefeldt, 2002: The shallow thermohaline circulation of the Indian Ocean. *Prog. Oceanogr.,* **53,** 57–103.

Schott, F. A., S.-P. Xie, and J. P. McCreary, 2009: Indian Ocean circulation and climate variability. *Rev. Geophys.,* **47,** RG1002, doi:10.1029/2007RG000245.

Song, X., and G. Zhang, 2009: Convection parameterization, tropical Pacific double ITCZ, and upper-ocean biases in the NCAR CCSM3. Part I: Climatology and atmospheric feedback. *J. Climate,* **22,** 4299–4315.

Taylor, K. E., J. S. Ronald, and G. A. Meehl, 2012: An overview of CMIP5 and the experiment design. *Bull. Amer. Meteor. Soc.,* **93,** 485–498.

Ummenhofer, C. C., A. S. Gupta, P. R. Briggs, M. H. England, P. C. McIntosh, G. A. Meyers, M. J. Pook, M. R. Raupach, and J. S. Risbey, 2011: Indian and Pacific Ocean influences on southeast Australian drought and soil moisture. *J. Climate,* **24,** 1313–1336.

Uppala, S. M., and Coauthors, 2005: The ERA-40 re-analysis. *Q. J. R. Meteor. Soc.,* **131,** 2961–3012.

Vecchi, G. A., and B. J. Soden, 2007: Global warming and the weakening of the tropical circulation. *J. Climate,* **20,** 4316–4340.

Wahl, S., M. Latif, W. Park, and N. Keenlyside, 2011: On the tropical Atlantic SST warm bias in the Kiel climate model. *Climate Dyn.,* **36,** 891–906.

Wang, C., L. Zhang, S.-K. Lee, L. Wu, and C. R. Mechoso, 2014: A global perspective on CMIP5 climate model biases. *Nature Climate Change,* **4,** 201–205.

Webster, P. J., A. M. Moore, J. P. Loschnigg, and R. R. Leben, 1999: Coupled ocean-atmosphere dynamics in the Indian Ocean during 1997-98. *Nature,* **401,** 356–360.

Weller, E., and W. Cai, 2013a: Asymmetry in the IOD and ENSO teleconnection in a CMIP5 model ensemble and its relevance to regional rainfall. *J. Climate,* **26,** 5139–5149.

Weller, E., and W. Cai, 2013b: Realism of the Indian Ocean Dipole in CMIP5 models: The implications for climate projections. *J. Climate,* **26,** 6649–6659.

Wittenberg, A. T., A. Rosati, N.-C. Lau, and J. J. Ploshay, 2006: GFDL's CM2 global coupled climate models. Part III: Tropical Pacific climate and ENSO. *J. Climate,* **19,** 698–722.

Wyrtki, K., 1973: An equatorial jet in the Indian Ocean. *Science,* **181,** 262–264.

Xie, S.-P., H. Annamalai, F. A. Schott, and J. P. McCreary, 2002: Structure and mechanisms of South Indian Ocean climate variability. *J. Climate,* **15,** 864–878.

Xie, S.-P., K. Hu, J. Hafner, H. Tokinaga, Y. Du, G. Huang, and T. Sampe, 2009: Indian Ocean capacitor effect on Indo-western Pacific climate during the summer following El Nino. *J. Climate,* **22,** 730–747.

Yamagata, T., S. K. Behera, J.-J. Luo, S. Masson, M. Jury, and S. A. Rao, 2004: Coupled ocean-atmosphere variability in the tropical Indian Ocean in Earth's Climate: The Ocean-Atmosphere Interaction. In *Geophys. Monogr. Ser.*, edited

by Wang, C., S.-P. Xie, and J. A. Carton, 189–211, vol. 147, American Geophysical Union, Washington, D.C., USA.

Yang, J., Q. Liu, S.-P. Xie, Z. Liu, and L. Wu, 2007: Impact of the Indian Ocean SST basin mode on the Asian summer monsoon. *Geophys. Res. Lett.,* **34,** L02708, doi:10.1029/2006GL028571.

Yu, J.-Y., and C. R. Mechoso, 1999: Links between annual variations of Peruvian stratocumulus clouds and of SST in the eastern equatorial Pacific. *J. Climate,* **12,** 3305–3318.

Zhang, G. J., and H. Wang, 2006: Toward mitigating the double ITCZ problem in NCAR CCSM3. *Geophys. Res. Lett.,* **33,** L06709, doi:10.1029/2005GL025229.

Zheng, X.-T., S.-P. Xie, G. A. Vecchi, Q. Liu, and J. Hafner, 2010: Indian Ocean dipole response to global warming: Analysis of ocean-atmospheric feedbacks in a coupled model. *J. Climate,* **23,** 1240–1253.

Zheng, X.-T., S.-P. Xie, Y. Du, L. Liu, G. Huang, and Q. Liu, 2013: Indian Ocean Dipole response to global warming in the CMIP5 multi-model ensemble. *J. Climate*, **26,** 6067–6080.

Zheng, Y., J.-L. Lin, and T. Shinoda, 2012: The equatorial Pacific cold tongue simulated by IPCC AR4 coupled GCMs: Upper ocean heat budget and feedback analysis. *J. Geophys. Res.,* **117,** C05024, doi:10.1029/2011JC007746.

Table 1. A list of the 19 CMIP5 CGCMs used in this study and the labels to denote them in the figures and text.

Model name	Model group (or center)	Label
ACCESS1-0	CSIRO	M1
CanESM2	CCCma	M2
CCSM4	NCAR	M3
CNRM-CM5	CNRM/CERFACS	M4
CSIRO-Mk3.6	CSIRO/QCCCE	M5
FGOALS-S2	IAP	M6
GFDL-ESM2G	NOAA GFDL	M7
GFDL-ESM2M	NOAA GFDL	M8
GISS-E2-R	NASA GISS	M9
HadGEM2-CC	MOHC	M10
HadGEM2-ES	MOHC	M11
INMCM4	INM	M12
IPSL-CM5R-LR	IPSL	M13
IPSL-CM5R-MR	IPSL	M14
MIROC5	JAMSTEC	M15
MPI-ESM-LR	MPI-M	M16
MPI-ESM-MR	MPI-M	M17
MRI-CGCM3	MRI	M18
NorESM1-M	NCC	M19

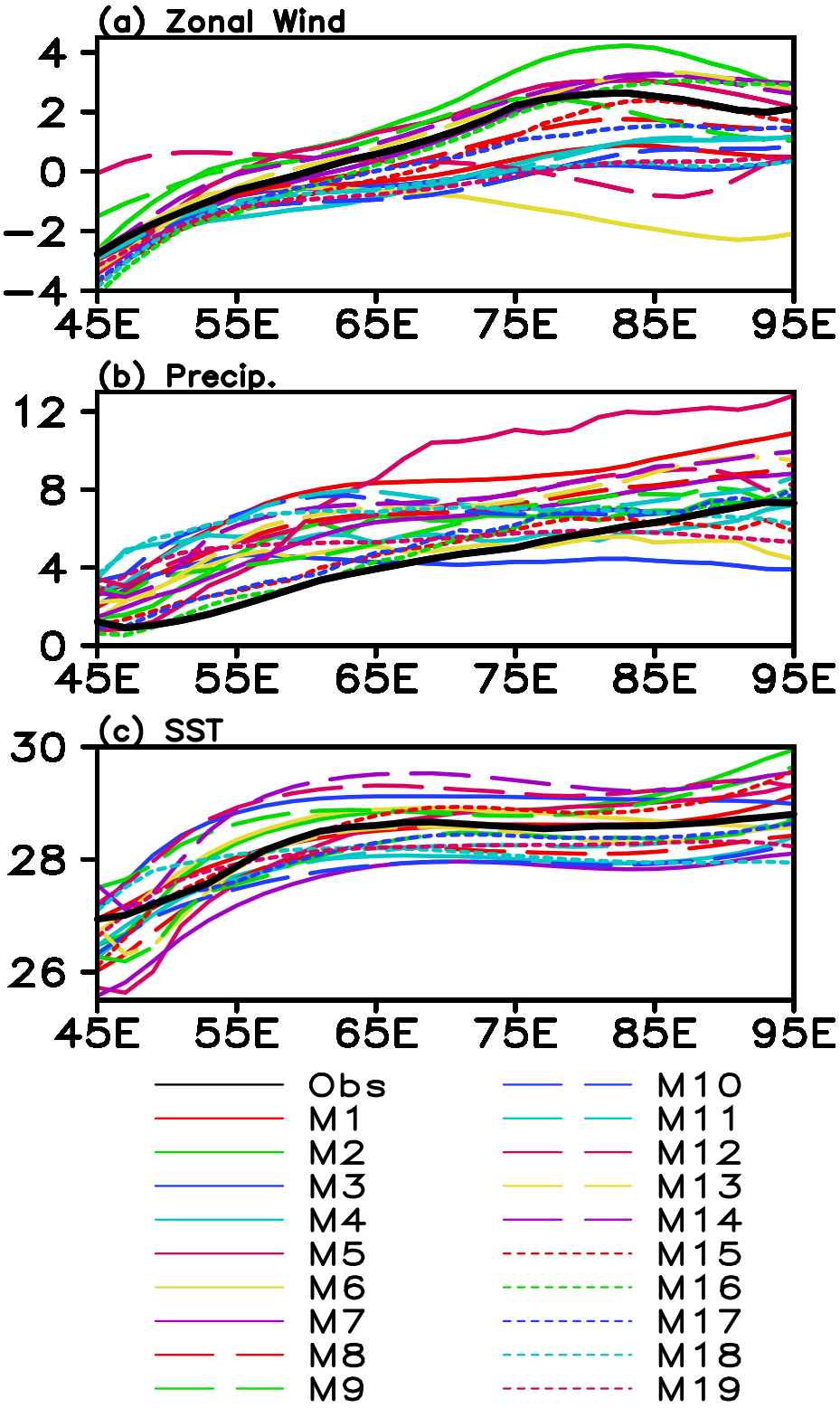

Figure 1. Zonal sections of annual mean (a) zonal wind (m/s), (b) precipitation (mm/day), and (c) SST (°C) along the equator in observations (black line) and 19 CMIP5 CGCMs (colored lines).

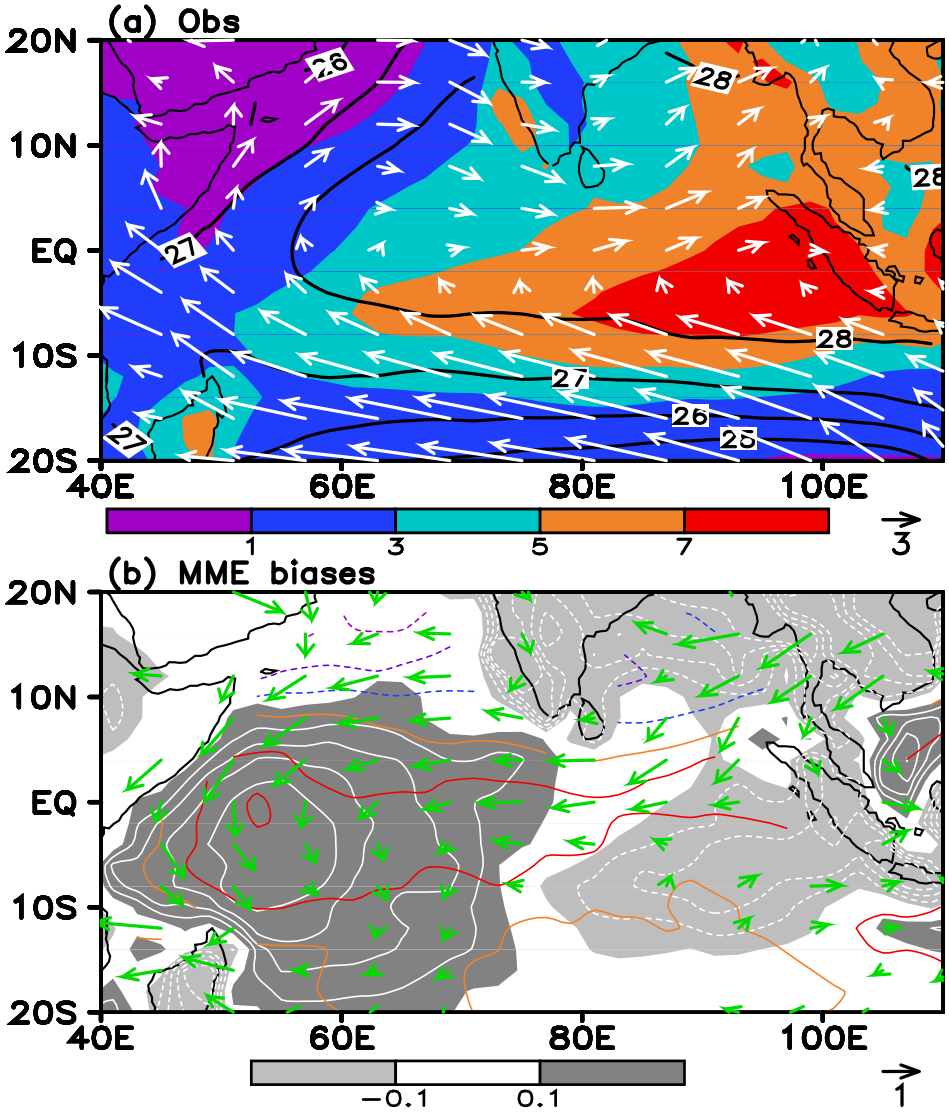

Figure 2. (a) Annual mean 925 mb wind (vectors, m/s), precipitation (color shaded, mm/day), and SST (black contours, °C) in observations; (b) The multi-model ensemble mean (MME) biases of annual mean 925 mb wind (vectors), precipitation [gray shaded and white contours, contour interval (CI) 0.1], and SST (color contours, CI 0.01) in 19 CMIP5 CGCMs. The precipitation and SST for observations and each CGCM in (b) are normalized by their tropical IO (40°-110°E, 20°S-20°N) means. The wind speed smaller than 0.6 m/s and 0.3 m/s in (a) and (b) has been masked out, respectively.

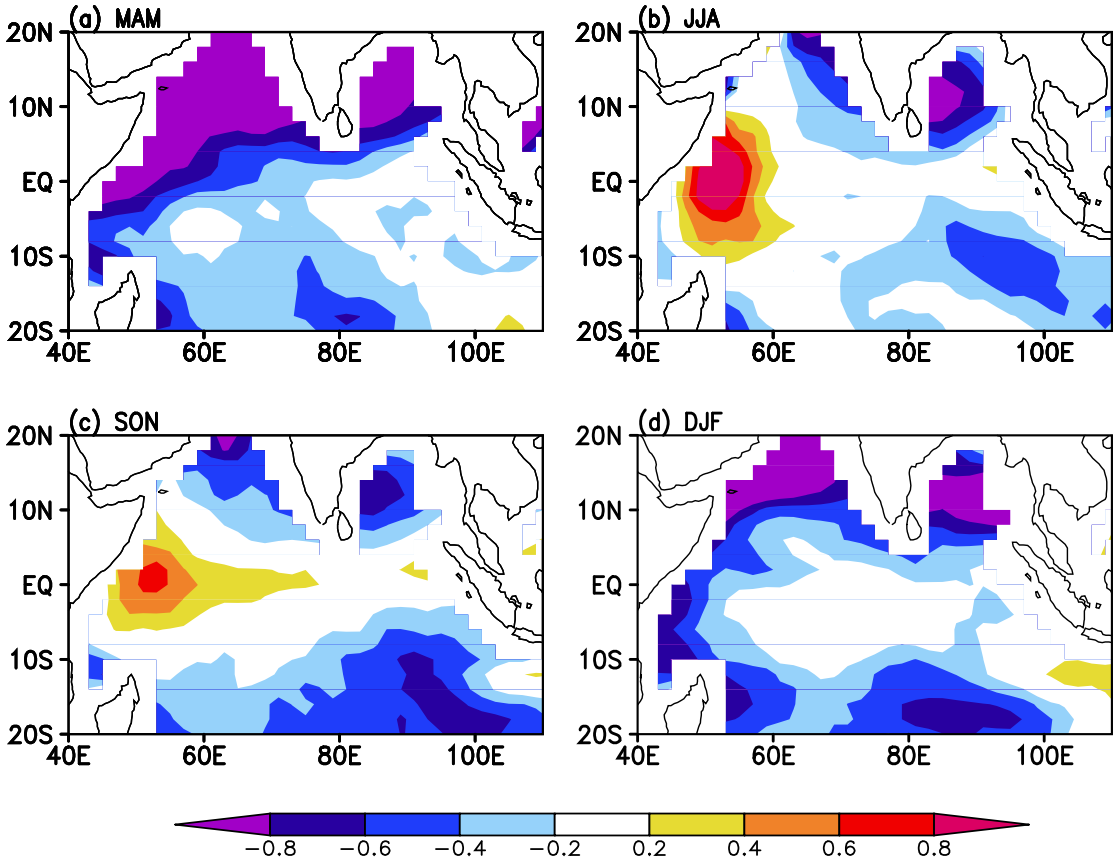

Figure 3. The MME biases of seasonal SST (°C) in boreal (a) spring (March-May, MAM), (b) summer (June-August, JJA), (c) autumn (September-November, SON), and winter (December-February, DJF) in 19 CMIP5 CGCMs.

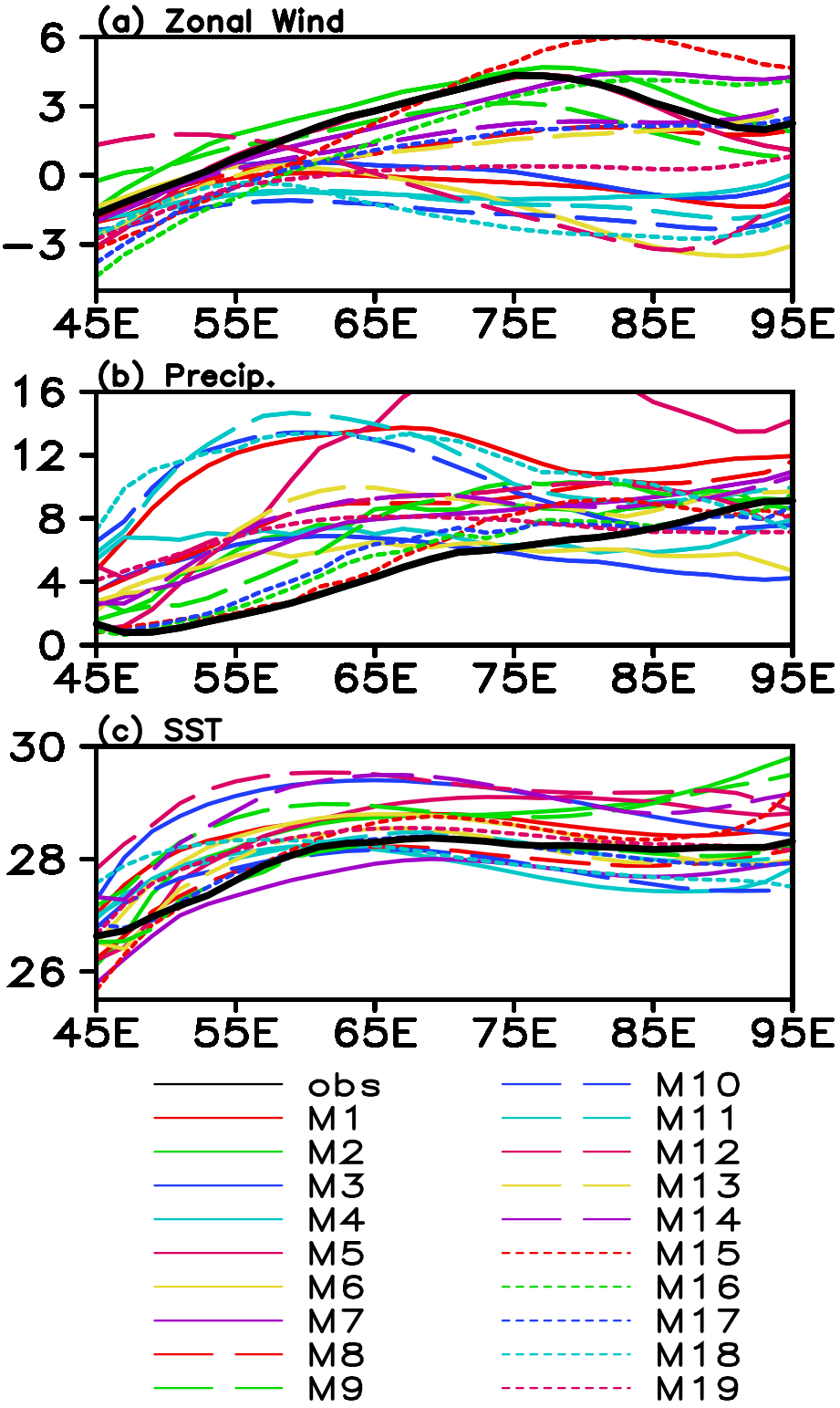

Figure 4. Same as Figure 1, but for June-November.

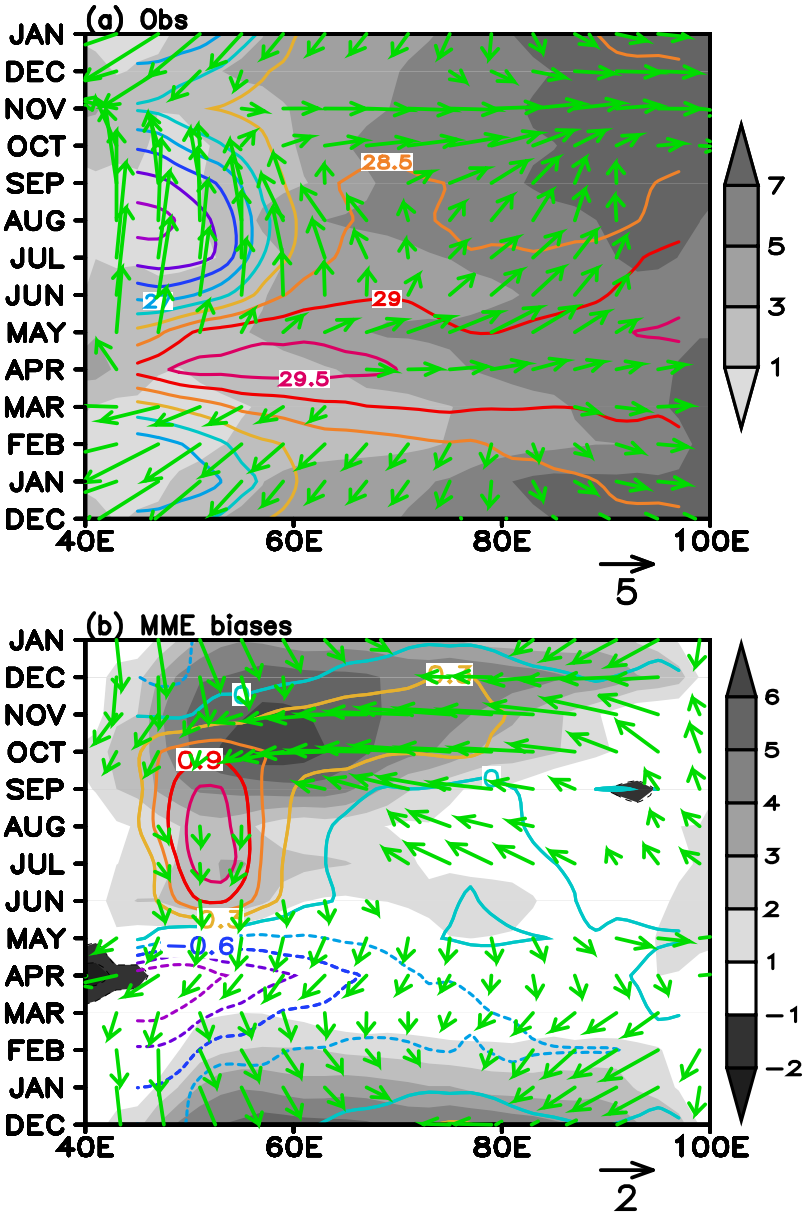

Figure 5. (a) Longitude-time section of the observed climatologies of 925 mb wind (vectors, m/s), precipitation (gray shaded, mm/day), and SST (color contours, °C) on the equator; (b) Same as (a), but for the MME biases in 19 CMIP5 CGCMs. The wind speed smaller than 2.0 m/s and 0.8 m/s has been masked out in (a) and (b), respectively.

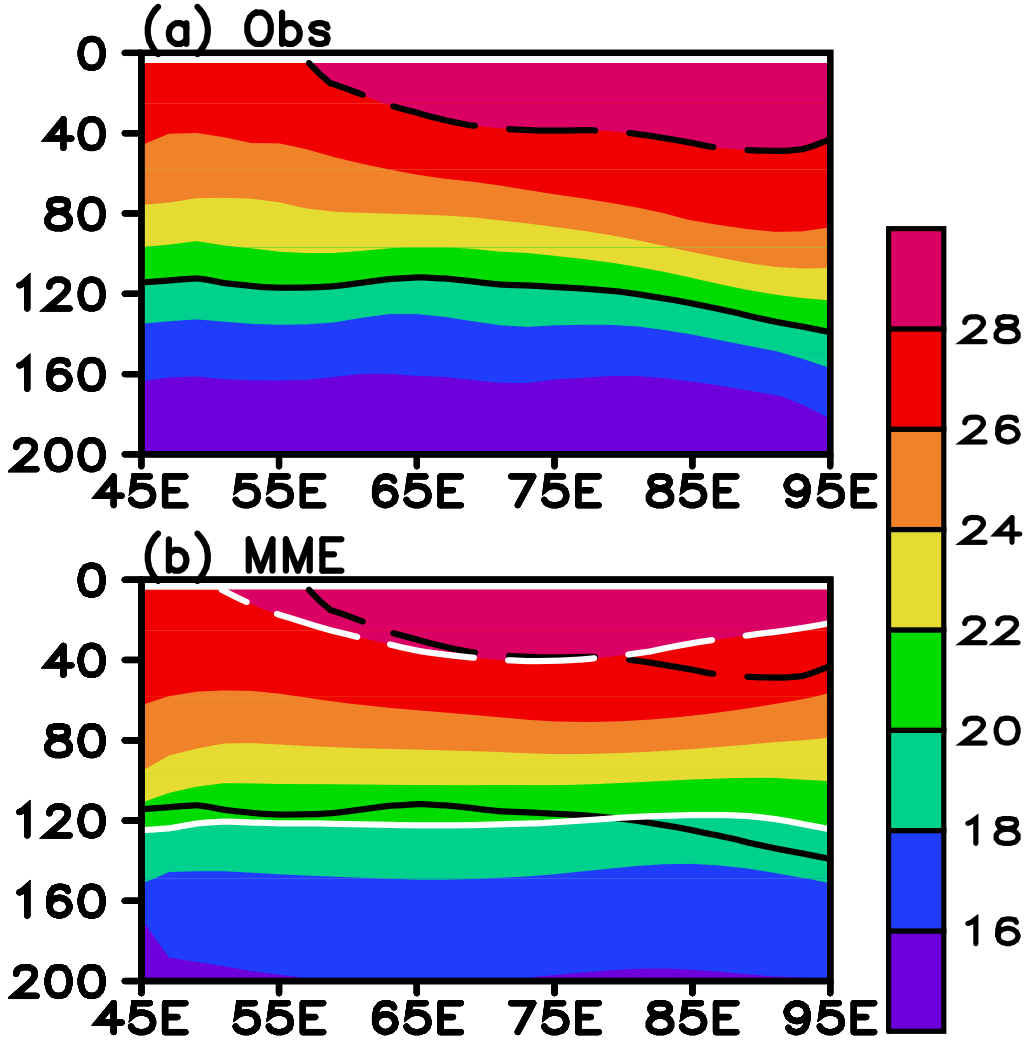

Figure 6. Ocean temperature (color shaded, °C) in the zonal-vertical plane along the equator during SON in (a) observations and (b) the MME simulation. The 20 °C isotherms in observations and the MME simulation are denoted by the black and white solid curves, respectively. The 28 °C isotherms in observations and the MME simulation are denoted by the black and white dashed curves, respectively.

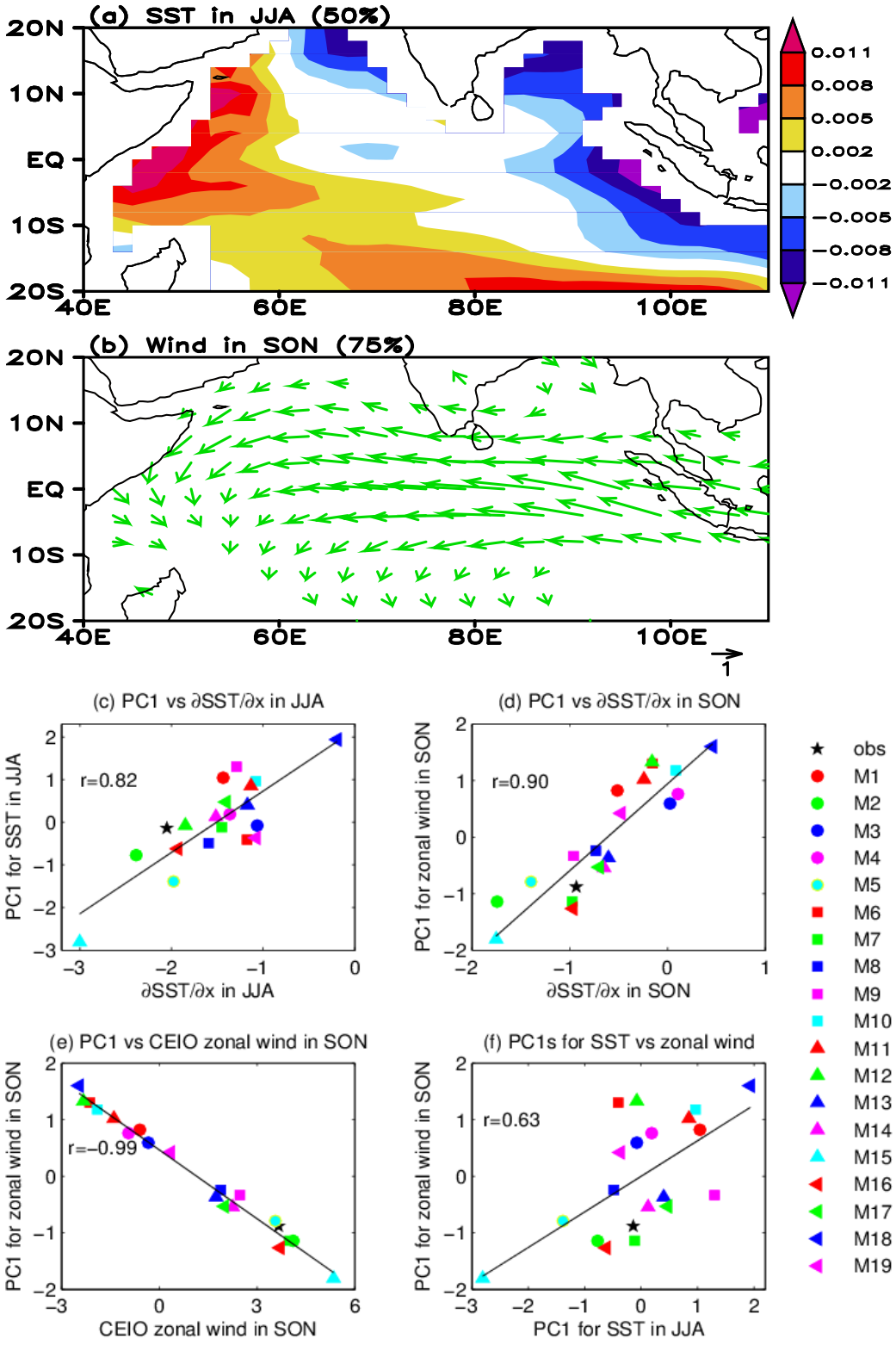

Figure 7. (a) The regression pattern of the first inter-model EOF mode for the JJA SST in the equatorial IO (40°-100°E, 6°S-6°N) among observations and 19 CMIP CGCMs (accounting for 50% of the total variance). Here the SST for observations

and each CGCM is normalized by their tropical IO (40°-110°E, 20°S-20°N) means; (b) Same as (a), but for the SON zonal wind (accounting for 75% of the total variance); (c) Scatter plot of the first principal component (PC1) for the JJA SST versus west-east JJA SST gradient (40°-60°E minus 80°-100°E) on the equator; (d) Same as (c), but for the PC1 for the SON zonal wind versus west-east SON SST gradient; (e) Same as (c), but for the PC1 for the SON zonal wind versus central equatorial IO (CEIO, 70°-90°E) SON zonal wind; (f) Same as (c), but for the PC1s for the JJA SST and SON zonal wind. The inter-model correlation (r) is shown in each panel of (c)-(f).

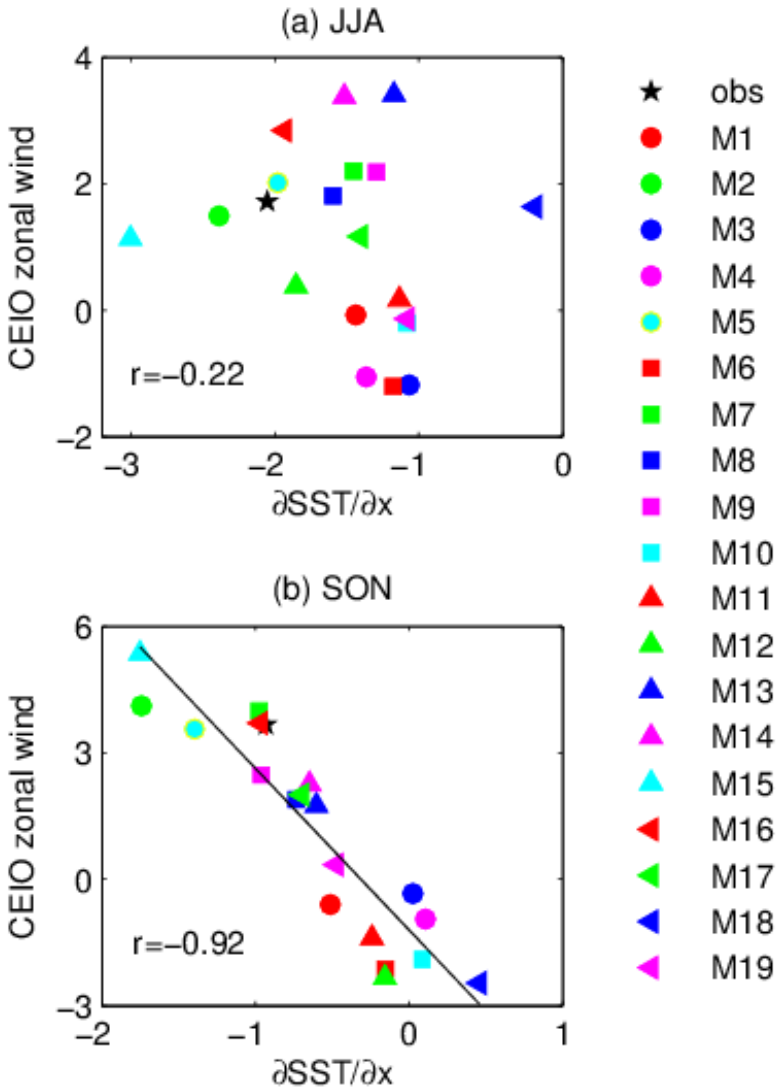

Figure 8. Scatter plots of the west-east SST (°C) gradient along the equatorial IO versus CEIO zonal wind (m/s) among observations and 19 CMIP CGCMs during (a) JJA and (b) SON. The inter-model correlation (r) is shown in the left-lower side of each panel.

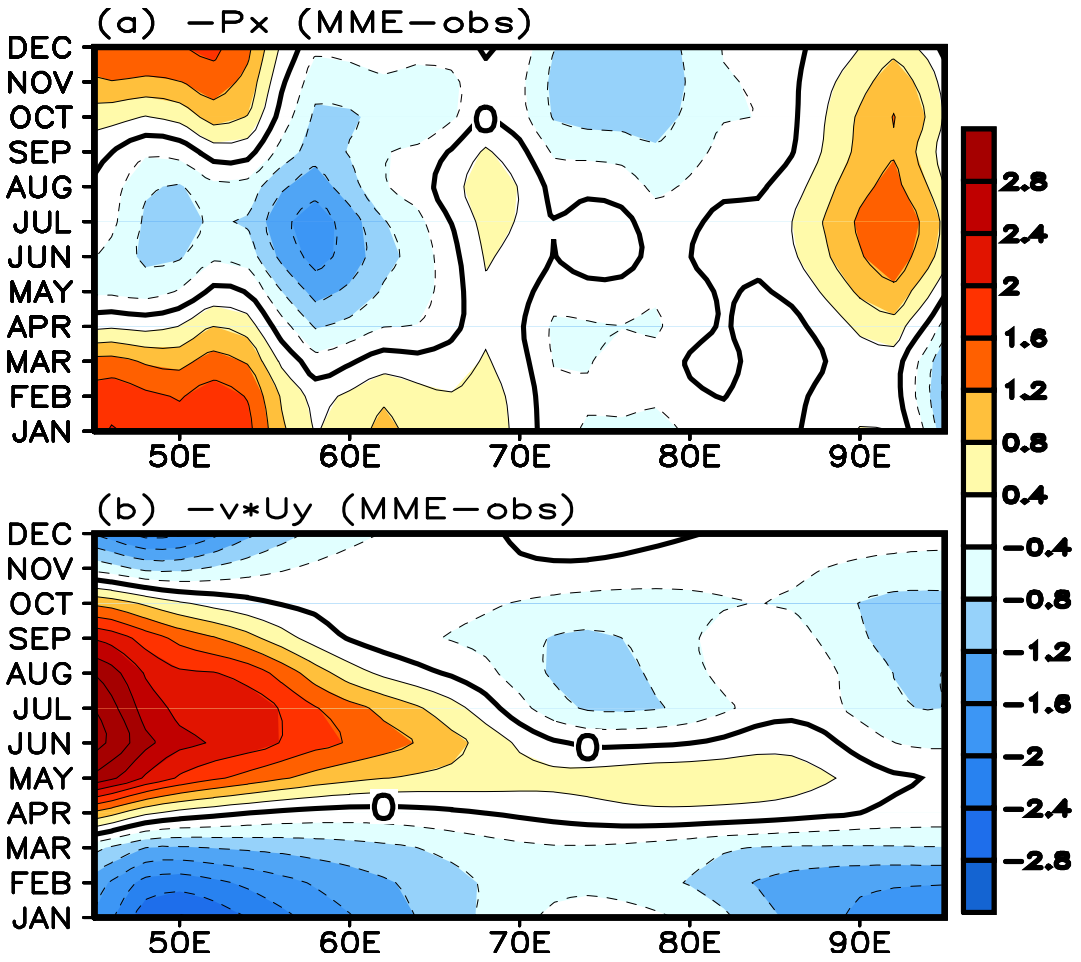

Figure 9. Longitude-time sections of MME biases for the (a) pressure gradient term (m/s^2) and (b) meridional momentum advection term (m/s^2) in Equation (2) on the equator in 19 CMIP5 CGCMs.

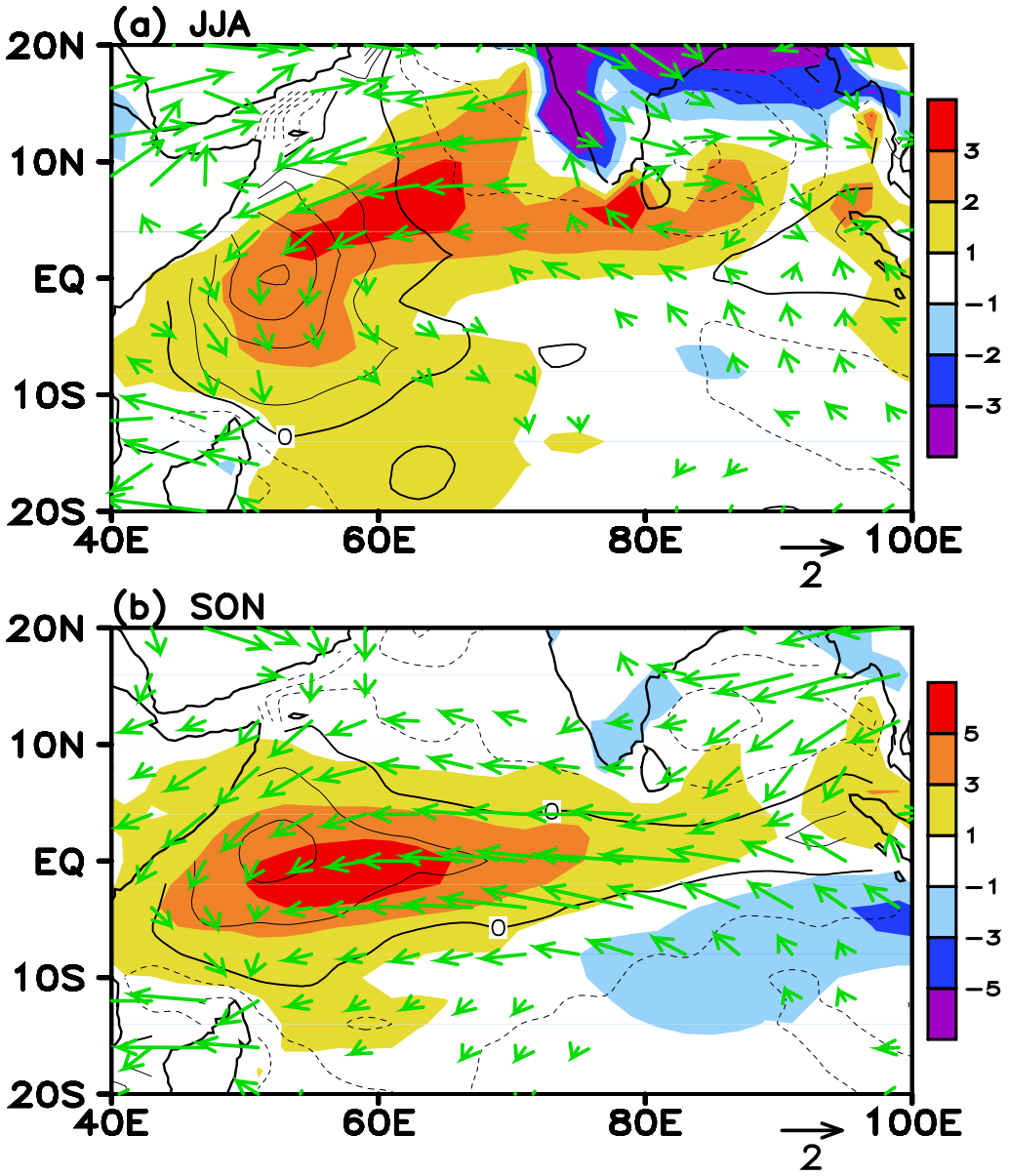

Figure 10. (a) The MME biases of 925 mb wind (vectors, m/s), precipitation (colored shaded, mm/day), and SST (CI: 0.3 °C) in JJA in 19 CMIP5 CGCMs; (b) Same as (a), but in SON. The wind speed smaller than 0.5 m/s has been masked out.

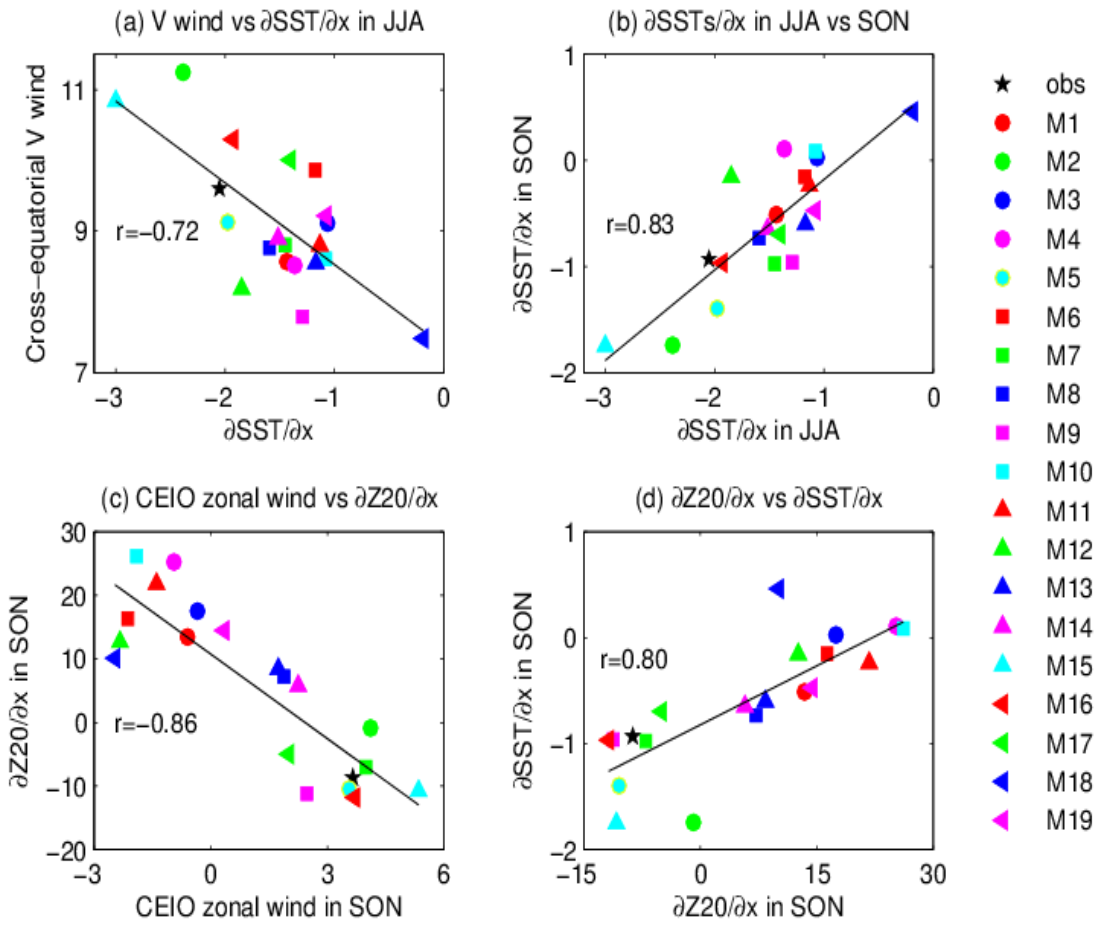

Figure 11. Scatter plots of (a) the meridional wind (m/s) in the equatorial western IO (40°-60°E) versus west-east SST (°C) gradient in JJA along the equator, (b) the SST gradients in JJA versus SON; (c) the CEIO zonal wind (m/s) versus west-east z20 (m) gradient in SON, and (d) the z20 versus SST gradients in SON. The inter-model correlation (r) is shown in each panel.

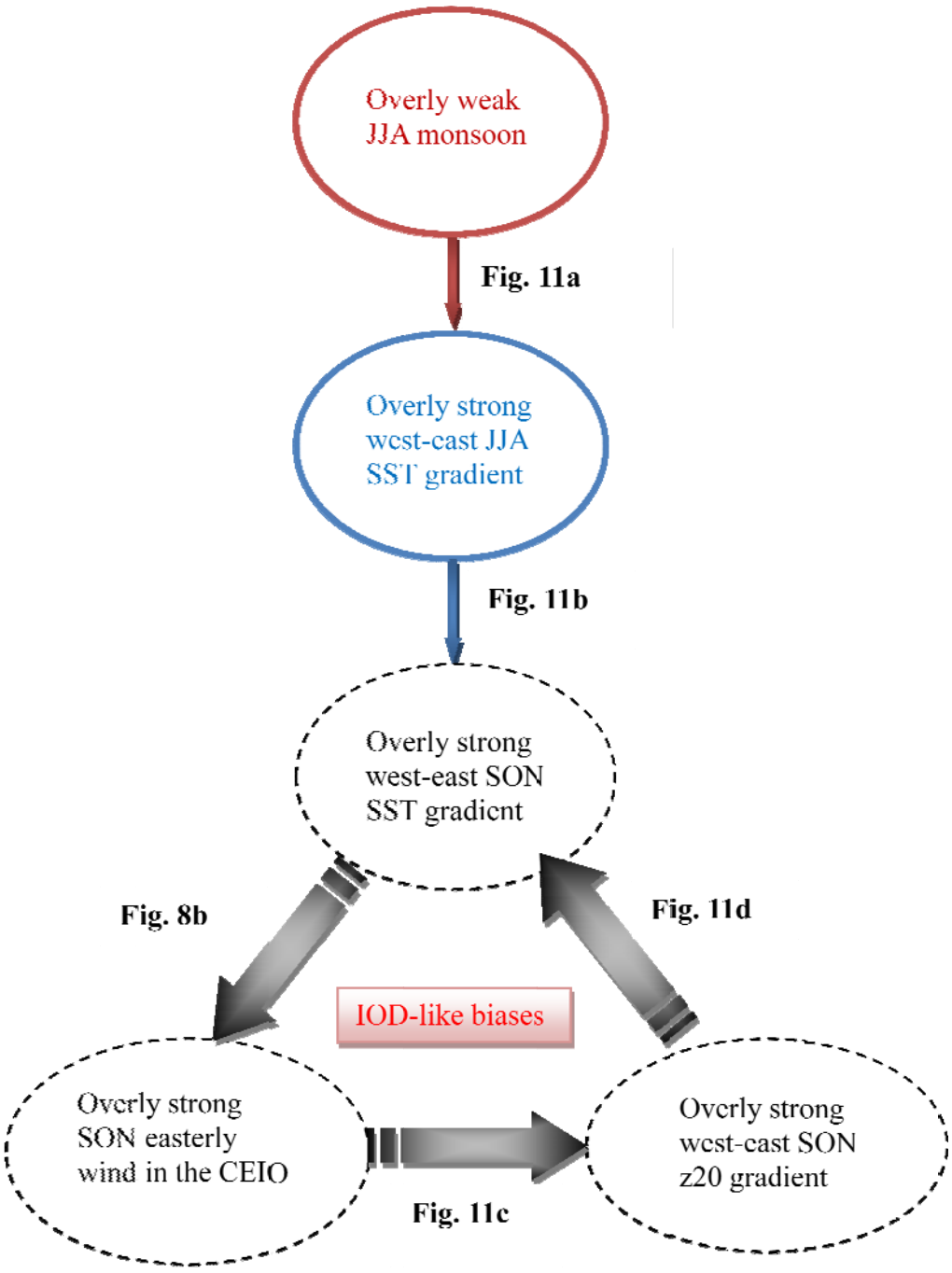

Figure 12. Schematic showing the South Asian summer monsoon origin and Bjerknes feedback for the seasonal evolutions of IOD-like bias pattern in CMIP5 CGCMs.

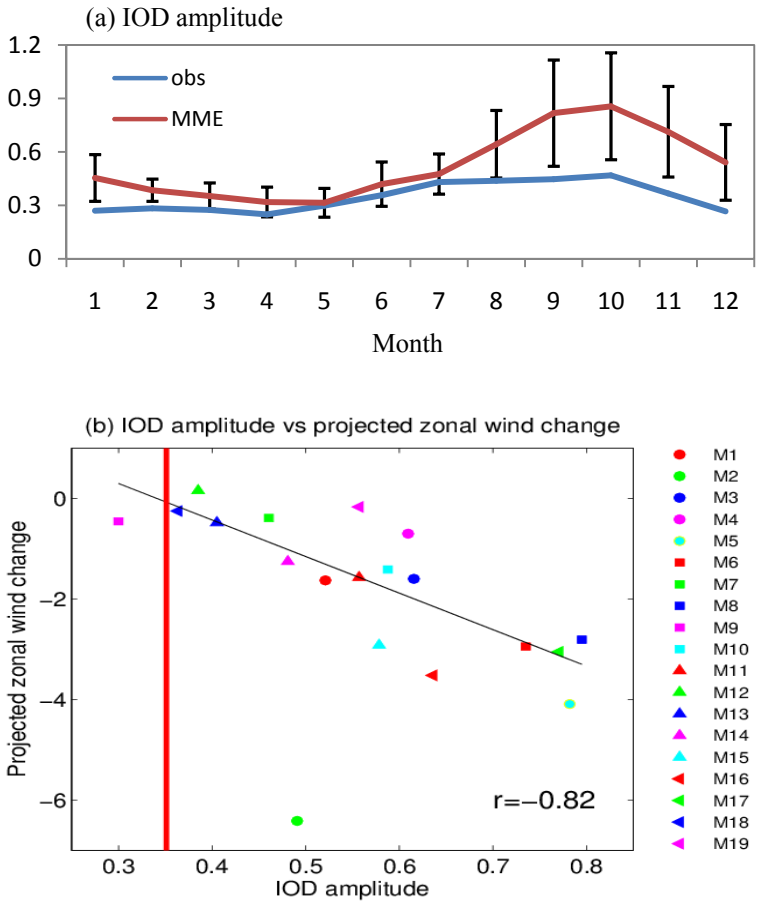

Figure 13. (a) Comparison of monthly IOD amplitudes between observations and the MME simulation; (b) Scatter plot of the simulated IOD amplitude versus projected zonal wind change in the CEIO for SON under global warming in 19 CMIP5 CGCMs. The IOD amplitude is defined as the standard deviation of Dipole Mode index (DMI) proposed by Saji et al. (1999). The error bars in (a) indicate the standard deviation spread among CMIP5 CGCMs. The red line in (b) denotes the observed IOD amplitude. The inter-model correlation (r=-0.82) is shown in (b) with one outlier (M2) excluded.